

Hyperspectral mapping of crop and soils for precision agriculture

Michael L. Whiting*¹, Susan L. Ustin¹, Pablo Zarco-Tejada²,
Alicia Palacios-Orueta³, and Vern C. Vanderbilt⁴

¹CalSpace Center of Excellence, University of California,
One Shields Avenue, The Barn, Davis, CA 95616-8527 USA

²Instituto de Agricultura Sostenible, Consejo Superior de
Investigaciones Científicas, Córdoba, Espana.

³Escuela Tecnica Superior de Ingenieros de Montes,
Universidad Politecnica de Madrid, Madrid, Espana.

⁴NASA Ames Research Center, Moffett Field, CA, USA.

ABSTRACT

Precision agriculture requires high spectral and spatial resolution imagery for advanced analyses of crop and soil conditions to increase environmental protection and producers' sustainability. GIS models that anticipate crop responses to nutrients, water, and pesticides require high spatial detail to generate application prescription maps. While the added precision of geo-spatial interpolation to field scouting generates improved zone maps and are an improvement over field-wide applications, it is limited in detail due to expense, and lacks the high precision required for pixel level applications. Multi-spectral imagery gives the spatial detail required, but broad band indexes are not sensitive to many variables in the crop and soil environment. Hyperspectral imagery provides both the spatial detail of airborne imagery and spectral resolution for spectroscopic and narrow band analysis techniques developed over recent decades in the laboratory that will advance precise determination of water and bio-physical properties of crops and soils.

For several years, we have conducted remote sensing investigations to improve cotton production through field spectrometer measurements, and plant and soil samples in commercial fields and crop trials. We have developed spectral analyses techniques for plant and soil conditions through determination of crop water status, effectiveness of pre-harvest defoliant applications, and soil characterizations. We present the most promising of these spectroscopic absorption and narrow band index techniques, and their application to airborne hyperspectral imagery in mapping the variability in crops and soils.

Keywords: hyperspectral imagery, site-specific farming, narrow-band indexes, image spectroscopy

1. INTRODUCTION

Precision agriculture is a management strategy with the potential to integrate varied datasets through information technology in developing crop production decisions¹. The availability of GIS to aggregate and model yield data and crop status data collected near real time will promote increased efficiencies, and reduced producer costs and impact on the environment. In developing decision support tools for precision agriculture, the enhanced information for management within the field adds to an already complex decision process. Jones et al.² explore this complexity in structuring the information and decisions, while acknowledging there is imprecision within the process.

Moran et al.³ in a review of the state of precision crop management only a few years ago revealed some encouraging areas for the exploitation of remote sensing and the areas of severe limitation of existing systems. The expectation for remote sensing's greatest role is inputs to decision support systems for agronomic model calibration and validation. A future role for hyperspectral imagers is in crop diagnosis and soil physical and chemical characteristics. While remote sensing will not replace the soil and plant sampling entirely, the combination of imagery and local modeling and validation will improve producer efficiency if the soil and plant maps are provided within a short time period, near 24 hours for some applications such as irrigation⁴. Prediction of yield, plant stress, nutrient deficiencies, weed and insect infestations require timely applications of water, fertilizers and pesticides⁵. Combined with meteorological data, remote sensing on a region and local level will improve forecasting of the response of crops to management practices.

Unfortunately, advances in precision management are inhibited by the limitations in current satellites and airborne sensors: coarse spatial and spectral resolution, inadequate frequency of coverage, and long turn-around from acquisition to delivery. After several attempts from the commercial sector, the situation has changed little. The internet has greatly improved the potential speed of delivery to the grower, but the image sources remain limited. Both timeliness and expense remain the principal explanations for the lack of adoption. The economic scale to support the acquisition and analyses is for high value and large producers.

1.1 Spectroscopy techniques with hyperspectral data

With the high spectral resolution of hyperspectral imagery and field spectrometers, the basic spectroscopy techniques applied in lab analysis of organic and mineral spectra can be applied to agricultural landscapes in developing the layers for modeling the response of management practices by crops. Hyperspectral data also provides the most elemental form for convolving broad-bandwidths for simulating existing satellites, or determining the specific bands and widths for tuned-filter instruments.

Statistical relationships between the spectral region and variability in the image are often used to reduce data density through identifying specific bands that produce the greatest information content. Principal Component Analysis^{6, 7}, canonical analysis, and maximum-likelihood and others do not necessarily discover the physical rationale. From the determination of the most illustrative bands for the crop and soil characteristics, many two and three band indexes were developed using the broad-band satellite data, and were adapted to specific narrow spectral regions within the hyperspectral signature⁸. Band ratios have the advantage, when normalized, to improve comparability among band depths while reducing the variation not due to features of interest, but due to canopy and leaf geometry and sun angle. The most common techniques include Normalized Difference Vegetation Index (NDVI)⁹, Soil Adjusted Vegetation Index (SAVI)¹⁰ and many more shown in Table 1 after Zarco-Tejada et al.¹¹.

In controlled laboratory analyses, instruments produce smooth, high resolution spectra. As airborne and satellite imagers increase stability, the spectral quality for use in derivatives and other shape related techniques will increase. Meanwhile, techniques for reducing the noise, such minimum noise fraction greatly improve derivative and band-depth determinations, although at the expense of sensitivity to subtle narrow band variation¹². NIRA and principal component determination of the differences within the region of the spectra are standard techniques used in the laboratory^{6, 13}. Mineral and vegetation identification often employs the process of matching spectra from a library¹⁴. The process of Continuum Removal¹⁵ divides the spectrum by the background continuum, that normalizes absorption depths and shapes, making them easily comparable (Table 1). By normalizing both the example and target spectral, the variability in sun angle, surface geometry can be eliminated¹⁴. Tetracoder¹⁶ and commercial software exploit this technique for mineral and plant biochemical identification^{17, 18}. An alternative to fitting a spectrum to a library for identification is to model the shape of the absorption, then use the model parameters to predict the vegetation and soil composition or condition. One shape, the inverted Gaussian^{19, 20} fits the reflectance curve (Table 1). An advantage of the Gaussian over polynomial fitting is the few parameters used to describe the absorption, and which can be related to the identification and abundance of the absorber. Multiple Gaussian functions are used in series to model the shape of combination absorptions²¹.

1.2 Techniques in identifying soil characteristics

Each technique above has its strengths in soil classification, mineral, moisture, and nutrient determinations. Here are just few examples applying the techniques to determine soil types and condition. Early investigations using laboratory spectra determined moisture, clay, organic matter and iron contents were the primary chromophores²²⁻²⁵. Recent work by Chang et al.⁶ and Shepherd and Walsh²⁶ showed PCA and cluster analyses of laboratory spectra can separate Total C, total N, moisture, cation-exchange capacity (CEC), 1.5 MPa water, sand, silt, and extractable Ca and other soil components for large numbers of soil samples over diverse ecological regions.

Several investigators have demonstrated classification of tonal differences related to soil types through simple techniques as density slicing to classify soil types or characteristics using aerial photography²⁷, multispectral lab data²⁸ and SPOT imagery²⁹. In the right circumstances, multi-spectral photography and satellite imagery has been useful in differentiating organic matter and clay contents based on the tonal differences in the images^{30, 31}. Fontes and Carvalho³² using spectral conversion to Munsell colors demonstrated the relationship between iron content and specific absorptions

Table 1. Soil and Vegetation indexes for mineral and biochemical estimation calculated from multispectral and hyperspectral imagery.

Spectral Absorption Metrics	Equation	Reference
σ = shape parameter as defined by the inverted-Gaussian curve-fit model	$g(\lambda) = R\lambda_i + (R_{\min 500-600} - R_{\max 700-730})^* \exp\left(\frac{-(\lambda_i - \lambda_{\min 500-600})^2}{2\sigma^2}\right)$	Miller et al. (1990) ²⁰ , Bonham-Carter (1988) ¹⁹
Soil Moisture Gaussian Model (SMGM)	$g(\lambda) = R\lambda_i + (R_{2800} - R_{\max 1200-1800}) \exp\left(\frac{-(\lambda_i - \lambda_{2800})^2}{2\sigma^2}\right)$	Whiting et al. (2004) ³³
Continuum Removal Band Depth	$D_B = \frac{R_C - R_b}{R_C}$	Clark and Roush (1984) ¹⁵
Band depth Normalized on Center (BNC)	$D_n = D_B / D_C$	Kokaly and Clark (1999) ¹⁷
Band depth Normalized on Area (BNA)	$D_n = D_B / A$	Curran et al. (2001) ¹⁸

Structural Vegetation Indexes	Equation	Reference
Normalized Difference Vegetation Index (NDVI)	$NDVI = (R_{NIR} - R_{red}) / (R_{NIR} + R_{red})$	Rouse et al. (1974) ⁹
Modified Triangular Vegetation Index (MTVI1)	$MTVI1 = 1.2 * [1.2 * (R_{800} - R_{550}) - 2.5 * (R_{670} - R_{550})]$	Haboudane et al. (2004) ⁸
Modified Triangular Vegetation Index (MTVI2)	$MTVI2 = \frac{1.5 * [1.2 * (R_{800} - R_{550}) - 2.5 * (R_{670} - R_{550})]}{\sqrt{(2 * R_{800} + 1)^2 - (6 * R_{800} - 5 * \sqrt{R_{670}}) - 0.5}}$	Haboudane et al. (2004) ⁸
Renormalized Difference Vegetation Index (RDVI)	$RDVI = (R_{800} - R_{670}) / \sqrt{(R_{800} + R_{670})}$	Rougean and Breon, (1995) ³⁴
Simple Ratio Index (SR)	$SR = R_{NIR} / R_{red}$	Rouse et al. (1974) ⁹
Modified Simple Ratio (MSR)	$MSR = \frac{R_{NIR} / R_{red} - 1}{(R_{NIR} / R_{red})^{0.5} + 1}$	Chen (1996) ³⁵
Modified Chlorophyll Absorption in Reflectance Index (MCARI ₁)	$MCARI1 = 1.2 * [2.5 * (R_{800} - R_{670}) - 1.3 * (R_{800} - R_{550})]$	Daughtry et al. (2000) ³⁶
Modified Chlorophyll Absorption in Reflectance Index (MCARI ₂)	$MCARI2 = \frac{1.5 * [2.5 * (R_{800} - R_{670}) - 1.3 * (R_{800} - R_{550})]}{\sqrt{(2 * R_{800} + 1)^2 - (6 * R_{800} - 5 * \sqrt{R_{670}}) - 0.5}}$	Daughtry et al. (2000) ³⁶
Soil Adjusted Vegetation Index (SAVI)	$SAVI = (1+L) * (R_{800} - R_{670}) / (R_{800} + R_{670} + L)$ <p style="text-align: center;">[L ∈ (0,1)]</p>	Huete (1988) ¹⁰
Transformed Soil-Adjusted Vegetation Index (TSAVI)	$TSAVI = \frac{a(NIR - aRED - b)}{(NIR + aRED - b)}$	Baret et al. (1989) ³⁷
Modified SAVI with self-adjustment factor L (MSAVI)	$MSAVI = \frac{1}{2} \left[2 * R_{800} + 1 - \sqrt{(2 * R_{800} + 1)^2 - 8 * (R_{800} - R_{670})} \right]$	Qi et al. (1994) ³⁸
Optimized Soil-Adjusted Vegetation Index (OSAVI)	$OSAVI = (1 + 0.16) * (R_{800} - R_{670}) / (R_{800} + R_{670} + 0.16)$	Rondeaux et al. (1996) ³⁹

Chlorophyll Indexes	Equation	Reference
Transformed CARI (TCARI)	$TCARI = 3 \cdot [(R_{700} - R_{670}) - 0.2 \cdot (R_{700} - R_{550}) \cdot (R_{700} / R_{670})]$	Haboudane et al (2002) ⁴⁰
Triangular Vegetation Index (TVI)	$TVI = 0.5 \cdot [120 \cdot (R_{750} - R_{550}) - 200 \cdot (R_{670} - R_{550})]$	Broge and Leblanc (2000) ⁴¹
Photochemical Reflectance Index (PRI)	$PRI_1 = (R_{528} - R_{567}) / (R_{528} + R_{567})$ $PRI_2 = (R_{531} - R_{570}) / (R_{531} + R_{570})$	Gamon et al. (1992) ⁴²
Cellulose Adsorption Index (CAI)	$CAI = 0.5(R_{2020} + R_{2200}) - R_{2100}$	Daughtry et al.(1995) ⁴³

Vegetation Water Indexes	Equation	Reference
Normalized Difference Water Index (NDWI)	$NDWI = (R_{860} - R_{1240}) / (R_{860} + R_{1240})$	Gao, (1996) ⁴⁴
Simple Ratio Water Index (SRWI)	$SRWI = R_{858} / R_{1240}$	Zarco-Tejada et al., (2003) ⁴⁵
Shortwave Infrared Water Stress Index (SIWSI)	$SIWSI = \rho_6 - \rho_2 / \rho_6 + \rho_2$ $\rho_2 = 0.841 - 0.876$; $\rho_6 = 1.628 - 1.652$	Fensholt and Sandholt (2003) ⁴⁶
Plant Water Index (PWI)	$PWI = R_{970} / R_{900}$	Peñuelas et al. (1997) ⁴⁷

bands to clay minerals and organic matter in tropical soils. Soil taxonomic units were separated statistically by Palacios-Orueta and Ustin⁷ through PCA identification of those bands with the greatest explanation of the variance in lab data and Airborne Visible InfraRed Imaging Spectrometer (AVIRIS, NASA). Soil components of iron, organic matter, titanium oxide, aluminum oxide and silicate separated three major soil types in central Brazil using the 0.010 μm wavelengths of AVIRIS⁴⁸. Palacios-Orueta et al.⁴⁹ estimated organic matter and iron contents in coastal shrub land soils using a hierarchical foreground-background process.

Identifying specific mineral contents is possible with hyperspectral imagery through the mineral absorption position and depths^{14, 50, 51}. Clay and salt estimation techniques were applied to agricultural soils with AVIRIS and HyMap (HyVista, Inc., Sydney, AU) imagery by the continuum removal band depths^{52, 53}. There is a potential for applying narrow band techniques using broad-band imagery by fitting spectra to the general band center positions and cross-correlation to spectral references⁵⁴.

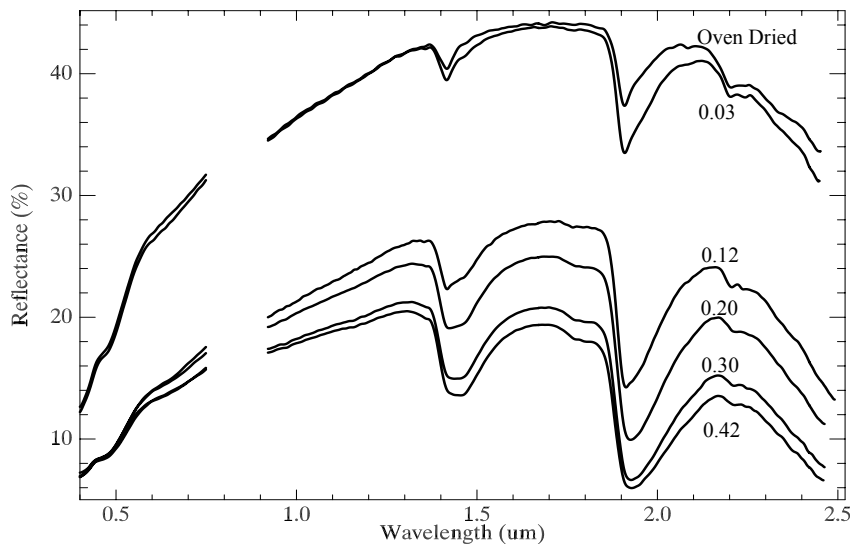


Figure 1. For this high clay content soil, the loss of albedo is a function of increasing gravimetric water content³³.

Moisture dramatically alters soil albedo, and thus, the mineral and organic matter spectral signatures. Water is a primary component among the many compositional variables in the soil surface interacting with the incident light. Bowers and Hanks⁵⁵ described the decrease in soil reflectance from the visible through the shortwave-infrared (0.4 – 2.5 μm), with increasing moisture, as shown in Figure 1. In the laboratory, many investigators have demonstrated that the water and clay bands are good predictors of water content⁵⁶⁻⁵⁸. Increasing moisture has a

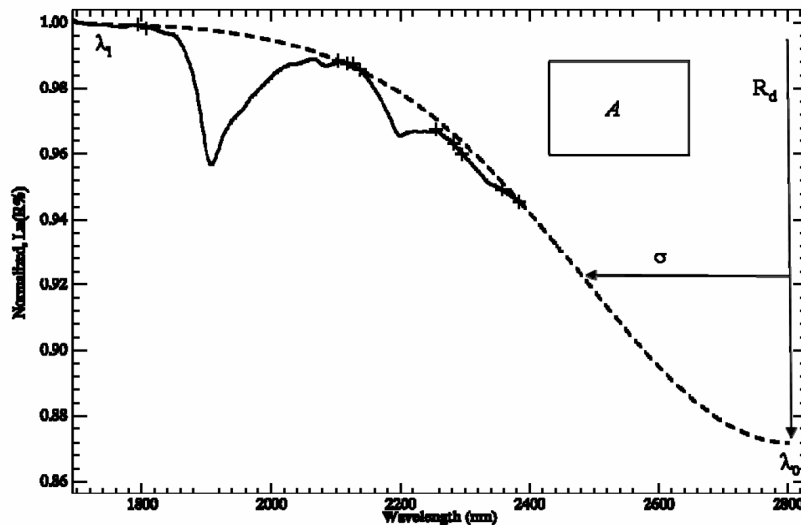


Figure 2. Water fundamental absorption influence on SWIR continuum modeled by fitting an inverted Gaussian function to the convex hull boundary points (+) from the position of maximum reflectance (λ_i) to the assigned water fundamental center (λ_0), with Gaussian amplitude (R_d) and distance to inflection (σ). The Gaussian area, above the spectrum, is denoted as A .³³

continuum is fitted with an inverted Gaussian distribution function after Miller et al.²⁰ in Table 1.

For two distinct Mediterranean regions of San Joaquin Valley California, USA, clayey soils, and Castilla-La Mancha, Spain, coarse textured, calcareous soils were spectrally measured through a sequence of gravimetric moisture contents from oven and air dry through saturation. Below field capacity, the model was highly predictive, estimating the water content within 2.7% (RMSE) with coefficient of determination (r^2) of 0.92 among both soil regions. When separated into landform position (Spain) and salinity (USA), estimates of the water content improved to between 1.7 to 2.5% (RMSE), with r^2 of 0.94 to 0.98 ($p < 0.001$).

Metternicht and Zinck⁵⁹ estimate that nearly 20% of all irrigated land globally is saline-affected. Management of water, seed and nutrients, and reclamation amendments, such as gypsum and sulfur, are substantial input costs to growers. Salinity mapping, especially with satellite images, has depended on plant indicators⁶⁰, generally due to the vigor or lack of vegetation cover. In cropped fields, the reduction of plant vigor is readily identified, multispectral bands using NDVI⁶¹. Saline and sodic soil reflectance revealed salt mineral (amorphous or crystal), and quantified through many common remote sensing procedures such a continuum absorption feature matching technique and plant indicators on ground measurements and hyperspectral (HyMap) images for segmenting of the salinity classes⁶².

1.3 Techniques in identifying crop characteristics

A number of promising techniques have been investigated for determining the crop stress due to the lack of nutrient and water, and the abundance pests. Nearly all the spectroscopy techniques described above have been applied to determine various crop conditions. An excellent review of techniques for estimating water stress in crops from hyperspectral images is presented by Moran et al.⁶³, Champagne et al.⁶⁴, and Downing et al.⁶⁵. Development of simulated spectra for agricultural crops under various conditions is enhanced by parameterizing the water content to Equivalent Water Thickness (EWT). Tucker⁶⁶ determined light absorption in the SWIR region (1.55 to 1.75 μm) for satellite measured reflectance was optimum for estimating the amount of water in the canopy.

Serrano et al.⁶⁷ demonstrated AVIRIS hyperspectral imagery has sufficient spectral resolution to accurately estimate the Relative Water Content (RWC, wet weight to dry matter weight), using the water band indexes such as Plant Water Index (PWI)⁴⁷ in chaparral community communities along the California coast. The best correlation to RWC were with indexes in the SWIR region, (WI, $r^2 = 0.38$, $p < 0.05$; Normalized Difference Water Index (NDWI)⁴⁴ ($r^2 = 0.44$, p

non-linear effect in decreasing albedo, and reducing the apparent strength of the absorption features of the minerals and organic matter^{56, 57}. In imagery, these water bands at 1.4 and 1.9 μm are susceptible to saturation by atmospheric water vapor measured by airborne and satellite platforms. To improve the accuracy of quantifying soil characteristics, the effects of varying soil moisture on hyperspectral images must be removed. Whiting et al.³³ fitted inverted Gaussian functions to the convex hull boundary points, transformed to natural log, in the shortwave-infrared (SWIR) region of a bare soil spectrum, Soil Moisture Gaussian Model (SMGM) (Table 1; Figure 2)³³. The function's variables with the greatest predictive value are the depth (amplitude) and the area above the spectral continuum. The

<0.001). The liquid water band absorptions in the SWIR were also well correlated with AVIRIS data⁶⁸. The use of water content is important in fuel load moisture contents in fire susceptible communities such forests and chaparral.

The change in vegetation reflectance in the visible region due to stress conditions is apparent by the changes in chlorophyll content as a function of metabolic change⁶⁹. NDVI and Simple Ratio Indexes (SR)⁹ are among the examples of band ratio indexes that exploit the relationship of chlorophyll absorption to the structural reflectance in the NIR region (Table 1). Gamon et al.⁴² presented the Photochemical Reflectance Index (PRI) from narrow band spectral would correlate with xanthophyll cycle pigments and the efficiency of photosynthesis, and nitrogen stress in sunflower canopies. From analysis of 490 bands in the visible region (0.35 - 1.05 μm), Thenkabail et al.⁷⁰ determined the optimum 12 bands for a tuned-filter instrument for estimating wet biomass, Leaf Area Index (LAI), yield (cotton), and canopy cover by comparing the broad-band NDVI, narrow band multiple-regression-determined selection of bands, and Transformed Soil-Adjusted Vegetation Index (TSAVI)³⁷ using cotton, soybeans, corn, and potatoes. The principle bands related to crop characteristics were greatest in the red (0.65 - 0.70 μm), next in the green (0.50 - 0.55 μm), and lastly with a narrow region of the NIR (0.90 - 0.94 μm). Notably, the band sensitive to moisture was centered on 0.98 μm . Blackburn⁷¹ used hyperspectral narrow bands to separate chlorophylls *a* and *b*, and carotenoids in bracken canopy. Though pigment-specific simple ratios related the concentration per unit area of individual pigments within the canopy, spectral derivatives of optical thickness (Log 1/R) were also closely associated with canopy pigment concentration, and were closer to estimating of concentration per unit mass of pigments both canopy and leaf.

Plant stress due to water, nutrients, and pest infestation reduce production, and are important indicators of yield. Regressions are still the primary method for calibrating the observed nutrient status and the image spectra⁷². Carter and Miller⁷³ used narrow bands, approximately 0.01 μm , within tuned-filter CCD imagery to determine image band centers for vegetation chemical stress at 420, 600, 670, 694, and 760 based on earlier research. Carter and Knapp⁷⁴ later linked plant stress to loss of chlorophyll, as 0.70 μm reflectance increases, as well as changes in the shorter wavelengths in green-yellow region. Kokaly and Clark¹⁷ demonstrated the potential for Continuum Removed band depth measurements by a high correlation to nitrogen status after water was removed. Using band depth methods, Curran et al. were also successful in estimating biochemical concentrations of total chlorophyll, nitrogen, cellulose, sugar, chlorophyll *a* and *b*, lignin and water contents¹⁸.

Due to the general effect of stress on vegetation as describe above, the common indexes, such as NDVI, when combined with strategic sampling, are effective in identifying regions within fields for managing insect infestations⁷⁵. Qin and Zhang⁷⁶ demonstrated blight stress could be determined in rice using multi-band airborne, and Zhang et al.⁷⁷ were successful in determining blight in tomatoes using hyperspectral imagery with Minimum Noise Fraction, before applying Spectral Angle Mapper⁷⁸ (ENVI, Research Systems, Inc., Boulder, CO, USA).

2. APPLICATIONS

2.1 Study area

The AZCAL management farms, in the southern San Joaquin Valley near the city of Lemoore in Kings County, California, are approximately mid-way between Los Angeles and San Francisco. The farms produce cotton, garlic, tomatoes, wheat, garbanzo beans, and pistachio nuts. Large quarter-section fields, approximately 64.8 ha, in a 9.2 km² area^{11, 53, 79}. Our studies over the past eight years concentrated on increasing the adoption of precision agriculture practices in cotton (*Gossypium hirsutum* L.) production. Among these remote sensing studies, we have investigated plant water stress indicators for timing irrigation, narrow-band indexes for anticipating yield, variable-rate applications of harvest aid chemicals, and for generating clay content maps as input to GIS prescription models.

2.2 Plant water contents and irrigation timing

Ustin et al.⁷⁹ showed absorptions depths at the 0.98 μm region indicated water content and stress by relating the index to the number of days since irrigation application. In this study, the effectiveness of using the band depth at 0.98 μm was compared to the more common band ratio methods of NDVI and NDWI. NDVI is dependent on chlorophyll absorption and is not sensitive to water content, and while leaf water does not absorb energy in the red and NIR bands. This index nonetheless has been used with multispectral airborne and satellite imagery for water determination.

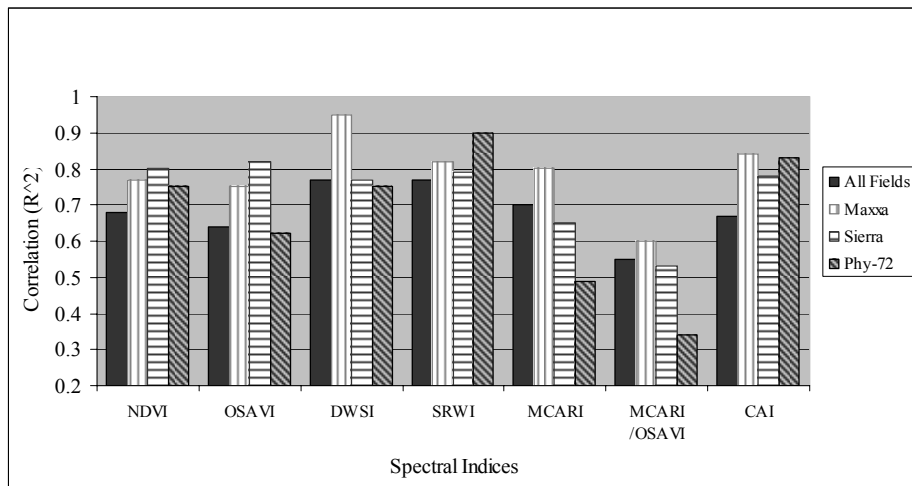


Figure 3. Regression coefficients (R^2) of the better indexes to trash among and within each cultivar.

Spectralon 99% reflectance standard panel (Labsphere, Inc, North Sutton, NH, USA), and post-processed using manufacturer's NIST calibration coefficients. In these three field campaigns, we collected 1584 canopy spectra to match whole plant water content and leaf water potential (pressure chamber) (7/23-25/05; 8/17-18/05; 9/07/05). The leaf reflectance and transmittance, and corresponding water content relative to leaf biomass and maximum water content were measured in 1893 samples (7/25/05; 8/17-18/05; 9/07/05; 10/4/05) using an integrating sphere (model 1800, LICOR Biosciences - Environmental, Lincoln, NE, USA) with the ASD spectrometer. The canopy equivalent water thickness (EWT) is a function of plant density and growth stage, which were measured by determining the number of plants in 2-m samples along the rows and mapping the plant structure (8/17-18/05). The relationship of LAI to cotton plant mapping is well established.

In initial analyses for the July 25 - 27, 2005 field campaign, there were no trends relating increasing water stress to NDVI, as measured by water content and leaf water potential (pressure chamber). This is reasonable since the visible and near infrared regions have a low sensitivity to short-term water stress. NDWI⁴⁴, PWI⁴⁷, and other common indexes also showed little or poor correlation to plant and leaf water content.

In previous years, we found some correlation between water stress and individual water absorption band depths⁷⁹ using continuum band depths, however, this season the correlations were poor. To improve the reliability of band depth indexes, the difference in leaf reflectance between the water band and its short or long wavelength shoulder were normalized following the methods used for NDVI and NDWI. The most successful were at PWI bands of 0.90 and 0.98 μm (NPWI) and the water bands in the NIR region at 1.08 and 1.14 μm (NPWI-2). Since the SWIR region of vegetation spectra is strongly related to water content⁶⁶, probably due to the water fundamental absorption at ca. 3.0 μm , water content could be estimated by the inverted Gaussian fitting algorithm SMGM³³. Each of these individual water band-depth ratios were individually correlated with whole leaf and whole plant water content, and leaf water potential, although poorly. However, by combining these water indexes, the canopy water content was well correlated. Water potential was predicted within 0.3 MPa RMSE ($R^2 = 0.66$), leaf water content within 2 g/g RMSE ($R^2 = 0.60$), and whole plant water content within 0.67 g/g RMSE ($R^2 = 0.54$; all p _values < 0.01).

2.3 Defoliation and reduced harvest aid chemical

Before harvesting cotton in the Southwest USA, this perennial plant is sprayed with herbicide, hormones, and desiccant chemicals, to shed leaves. Over past two years, 2004 and 2005, canopy spectral reflectance data was gathered during the early fall defoliation period while measuring the effectiveness of defoliation (desiccation, re-growth after treatment, and dry matter and water content). Our collaborators included University of California Cooperative Extension Specialists at the UC West Side Research and Extension Center (WSREC), and California State University Fresno researcher, and a commercial grower. The present methods for determining the timing and effectiveness of applications are through

During the 2005 season, the studies were conducted on three 65 ha (160 ac) fields during July, August, and September. Within each field, five plots were established using DGPS over the range of water stress levels from the maximum allowed by the grower just before irrigation to the minimum just after irrigation. Field spectral measurements were collected using a full range ASD Field Pro spectrometer (Analytical Spectral Devices, Boulder, CO, USA), calibrated to

visual estimation and ground measurements, such as Nodes Above Cracked Boll, % open bolls and the cut boll technique. Understanding and monitoring boll maturity is critical to obtaining high-quality lint.

Irrigation is shut off about a month before the harvest aid chemicals are applied, but residual plant and soil moisture varies over the fields, and this retards the effectiveness of the chemical applications. Determining the rate of defoliation will reduce unnecessary defoliant and residual chlorophyll staining in the cotton lint. To determine the most cost effective rates of applying harvest aid chemical, the chlorophyll and water content were monitored from before irrigation shutoff to the day before harvest, by measuring canopy reflectance using field spectrometers. These measurements will lead to developing image analysis techniques for site-specific defoliation management, and when combined with soil clay maps, identify specific areas within fields that can impact late season crop vigor and responsiveness to water, nutrient, or harvest aid management.

During 2004 the chemical applications were based on label recommendations, where during 2005 variable rates were applied on trial plots. At WSREC, the defoliation treatments were applied to three Acala cultivars (upland cotton), replicated over four randomly distributed 100 m by 4 m plots. Eight regularly spaced spectral measurements were collected along a longitudinal transect in each plot. These transects were repeated eight times between the two sites over the two week period following defoliant treatment four days after the first (9/22/04), and three (9/28/04), six (9/30/04), 10 (10/3/04), and 13 (10/6/04) days after the second treatment. The plant water and biomass measurements were made on three and 13 days after the second application, at the same time the overall yields, trash (non-lint) content, and other defoliation metrics within each trial plot were made. Fourteen spectral indexes, including structural, vegetation, water, cellulose and chlorophyll indexes, were calculated from the collected spectra. The index calculations were based on previous work by Zarco-Trejada et al.¹¹, and are among those in Table 1.

After post-processing the ground spectra with the Spectralon NIST coefficient data and eliminating anomalies, the spectral data were convolved to the wider band intervals of the NASA-AVIRIS sensor, then combined into "data cubes" as synthetic images. Initial processing was completed in ENVI software using band-math for common 14 vegetation spectral indexes and other classification schemes. The correlations between spectral indexes vary substantially through the defoliation period and between indexes and cultivars. The amount of trash predicted by the Simple Ratio Water Index (SRWI)⁴⁵ and Cellulose Adsorption Index (CAI)^{43, 80} for the absorption assigned to lignin at 2.1 μm . The CAI appears to be the most promising for all cultivars in accurately predicting trash levels (Figure 3). For example, structural indexes were generally mixed levels of correlation four days after the first defoliant was applied, but correlation improved after the second defoliant application for some cultivars. Structural indicators (i.e., leaf and plant density) included NDVI, Modified Triangular Vegetation Index (MTVI)⁸, Renormalized Difference Vegetation Index (RDVI)³⁴, and Optimized Soil-Adjusted Vegetation Index (OSAVI)³⁹. Water content indicators included band depth at 0.98 μm absorption, NDWI, SRWI, Shortwave Infrared Water Stress Index (SIWSI)⁴⁶, and SRWI. The chlorophyll content indicators included Modified Chlorophyll Absorption in Reflectance Index (MCARI)³⁶ and Transformed Chlorophyll Absorption Reflectance Index (TCARI)⁴⁰ and the cellulose indications based on the CAI. These indexes were then correlated to yield and trash (debris) content within four plot replicates for each of the three cultivars. The least squared mean fitted values to trash levels for structural indexes NDVI and OSAVI as the defoliation progresses are shown for a

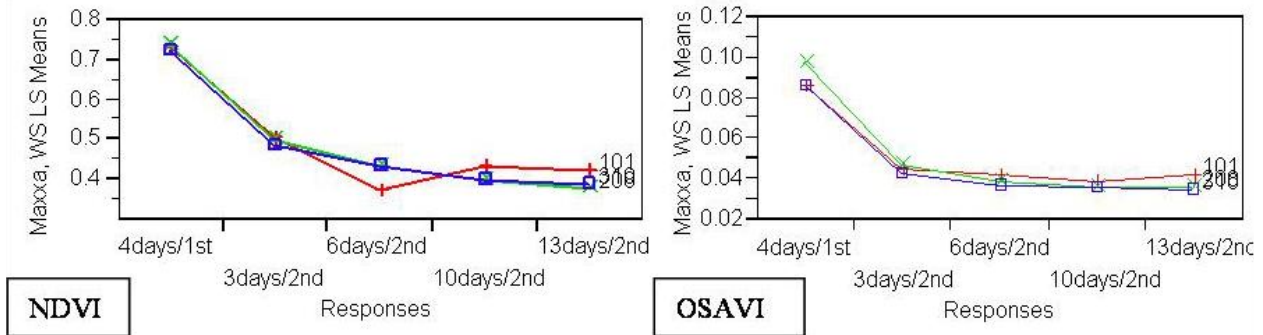


Figure 4. Comparison of common NDVI to OSAVI as indicators of trash content in harvested Maxxa upland cotton.

single cultivar Maxxa in Figure 4. Three trial plots indicated a rapid reduction of water, chlorophyll and amount of structure present. Inversely proportional with the other index categories, CAI showed an increase in the amount cellulose present over the course of the defoliation period.

2.4 Crop yield estimation in cotton

An important parameter in application rate decisions is early estimates of yield. Vegetation indexes from the decades of broad-band sensor research have been incorporated into hyperspectral methods for crop condition and yield estimation. Such indexes as NDVI are commonly used despite the demonstrated saturation of NDVI values at leaf area index (LAI) values above 3 and 4.

To determine the reliability of common indexes and a number of new narrow-band hyperspectral indexes to predict yield over time, hyperspectral visible and near infrared imagery for one field at our cotton field site was acquired nearly weekly for an entire growing season in 2001¹¹. Airborne Visible and Near InfraRed (AVNIR) hyperspectral sensor (OKSI, Inc., Torrance, CA, USA) images provided high spatial resolution of 1 m with 60 bands of 0.01 μm bandwidth from 0.43 μm to 1.01 μm . The yield data image provided by yield monitor and on-board computer software (Model AG700, AGRIplan, Stow, MA, USA) had a 4.5 m^2 resolution. After cross-calibrations among the images, the AVNIR data was resampled to the same spatial resolution of the yield monitor. The within-field variability of yield data was related to crop growth and canopy structure, chlorophyll concentration, water content and red-edge parameters. From these biophysical parameters, appropriate vegetation indexes were selected and their correlations to the gross cotton yield within each pixel through the different growth stages were compared. A *K means* clustering method was used to perform field segmentation on this temporal series of hyperspectral indexes in classes of low, medium and high yield, and confusion matrices used to calculate the kappa (κ) coefficient and overall accuracy.

Our results show that certain optical indexes and spatial yield variability are critically dependent on the growth stage, suggesting a potential for narrow band indexes at early and mid-growth stages will provide important crop management information¹¹. We found the best hyperspectral indexes for capturing yield variability were the structural indexes MTVI1, MTVI2⁸, NDVI⁹, RDVI³⁴, Modified Simple Ratio (MSR)³⁵, and OSAVI³⁹, and Modified SAVI (MSAVI)³⁸. The next group of indexes that performed well were the Chlorophyll Indexes Triangular Vegetation Index (TVI)⁴¹, MCARI1, MCARI2³⁶, and TCARI⁴⁰.

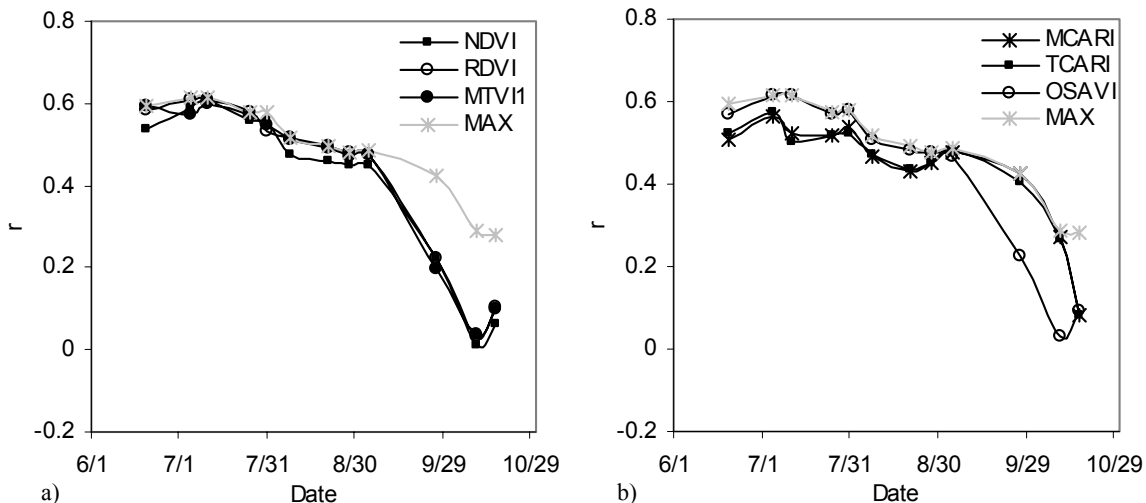


Figure 5. Correlation coefficients (r) obtained between spatial yield data and hyperspectral indices as function of time. The best correlation coefficient for any index is labeled MAX, compared with indices (a) NDVI, RDVI, MTVI1, (b) MCARI, TCARI, OSAVI¹¹.

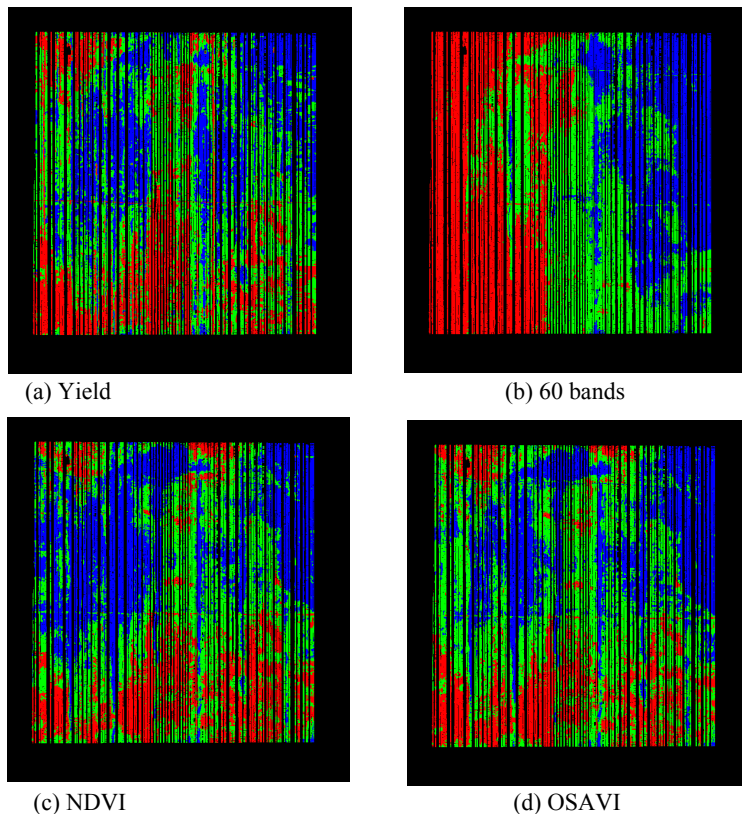


Figure 6. Unsupervised *K-means* clustering method for low (red), medium (green) and high yield (blue) classes calculated from the hyperspectral airborne image that obtained the highest correlation with yield (5 July 2001)¹¹.

The three classes were segmented in the yield and index images using K-Means classes. For the yield image (Figure 6a), from a principal component analysis for the most descriptive 60 reflectance bands (Figure 6b), NDVI (Figure 6c), and OSAVI (Figure 6d) for the time period of maximum prediction accuracy (5 July 2001). There is a slightly closer visual agreement between the yield segmentation and OSAVI than NDVI classes, which corresponds to the slightly better correlations, $r = 0.61$ and 0.59 , respectively. The use of PCA to select reflectance bands led to larger individual clusters in the classes, and less sensitive field segmentation, demonstrating that hyperspectral indices built on specific bands related to crop condition were better suited in this experiment for segmenting the field into zones of homogeneous yields for less precise management.

2.5 Soil surface mineral contents and moisture relationship

Greater spatial resolution in mapping mineral and organic matter contents contributes to improved modeling of plant and soil responses to various resource management and global changes in soil health, erosion, and desertification. Advances in precision farming require greater knowledge of the spatial heterogeneity in the mineral components to develop prescription models for water, nutrient, herbicide and pesticide applications, as well as improved management of nitrate and irrigation applications to reduce ground water pollution.

NASA collected AVIRIS data on 5 May 2002 over cotton fields near Lemoore, California⁵³. The images contain nominal 10 m pixels in 224 channels between the 0.40 μm to 2.50 μm , with a nominal 0.01 μm FWHM channel⁸¹. This image was atmospherically corrected using ACORN software (AGI, Boulder, CO, USA) and georectified by differentially corrected global positioning system (DGPS) measured image ground features. The affect of variable soil surface roughness on reflectance increases with salinity due to deflocculation by the sodium salt. The soil clods are less friable and there is greater horizontal orientation of the silts and clays before tillage. The productive and non-productive

In figure 5, the maximum correlation coefficient among all indexes obtained for each image date (MAX) is plotted along with the structural indexes NDVI, RDVI, MTVI1 (Figure 5a), and chlorophyll indexes MCARI, TCARI, OSAVI (Figure 5b) through time. Structural indices related to LAI (MCARI, MTVI, OSAVI) obtained the best relationships with yield and field segmentation at early growth stages. On the other hand, narrow-band indexes related to chlorophyll concentration and crop physiological status (MCARI, TCARI) were slightly better at later growth stages, close to harvest. The last irrigation was applied on 18 August 2001, before the 21 October 2001 harvest. The confusion matrices and class-analyses determined the highest overall accuracy (and kappa) for structural and chlorophyll indexes during the early stages was near 61% ($\kappa=0.39$) during July, dropping to 39% ($\kappa=0.08$) prior to harvest in October. MCARI chlorophyll index remained sensitive to within-field yield variability at late pre-harvest stage, obtaining overall accuracy of 51% ($\kappa=0.22$). The water indexes such as the NDWI, SRWI, PWI, and Gaussian parameters fitted to the red-edge were poor predictors of yield.

areas in the fields were separated for different regression models using a CIR composite of an earlier AVIRIS image, 28 August 1999, of the cropped fields that clearly show the variation in vigorous plants and no plants due to the high salinity (Figure 7a). A 5 May 2002 AVIRIS image of the bare soil fields was acquired after field preparation for spring planting, and before the first irrigation. The planting beds were shaped and surface aggregates were uniform. The productive and non-productive areas in the bare fields, and the roads and vegetated fields were masked separately before analysis using the interactive digitizer in the ENVI software. The sampling strategy can be seen in the 5 May 2002 AVIRIS image as white crosses where samples were collected in each of the adjacent nine pixels, Figure 7b. The registration accuracy of this image was within one pixel.

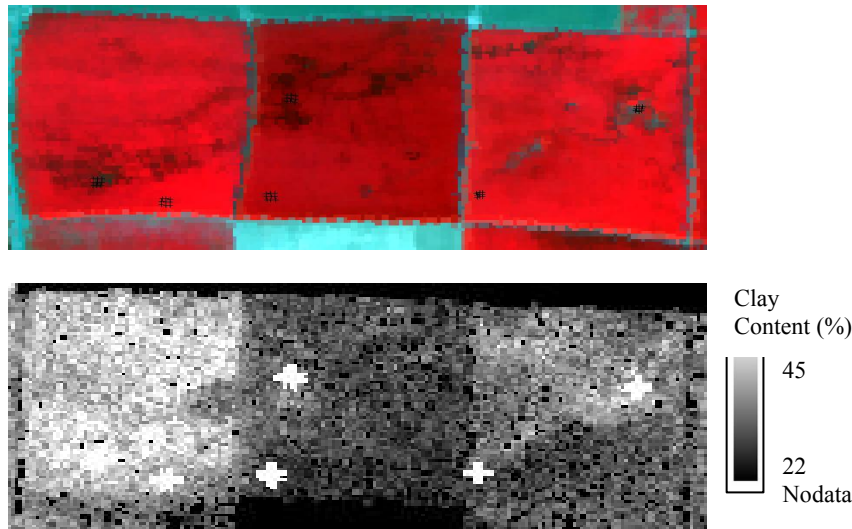


Figure 7 a) AVIRIS, 28 August 1999, false color infrared image (CIR) of full canopy cotton of Lemoore project site, b) AVIRIS image, 5 May 2002, in gray scale of clay contents of bare soil fields⁵³.

Registration and sample location inaccuracies were overcome by creating regions of interest (ROI) around ground reference data using a 3 x 3 pixel window. A weighted average spectrum was generated from the ROIs to extract nine spectra at each sample plot seen in Figure 7a and b. The influence of the salinity strata was included by selecting an equal number of samples, with two sites within each soil saline/non-saline strata. All three parameters, clay and carbonate continuum removed band depths and SMGM, were used as regressors in step-wise multiple regressions for predicting laboratory mineral contents⁵³. At Lemoore, smectite clay contents ranged from 22 - 43%, and these

secondary clay mineral absorptions were strong at $\sim 2.2 \mu\text{m}$.

In Lemoore, 53 samples were used to model clay content. The clay band depth alone was a poor predictor of clay content with $r^2 = 0.24$ and 4.0 % RMSE clay content. By combining the SMGM with the clay band depths, the R^2 doubled to approximately 0.51, and the RMSE decreased to 3.6 %. The difference in RMSE contributed by residual moisture in these air dried soils, approximately 4 to 8% water content, was approximately 0.4 % clay RMSE, or a 10% reduction in prediction error on a mean of 30.0 %. At air dry status, the SMGM, with these predominant clay soils, predicted clay content equally as well as the spectral band depth. With greater soil moisture, the SMGM is expected to improve the clay content estimates. Within these error estimates is the variability in the laboratory measurement and thus increases the spectral correlations. Having determined the mineral content model, the regression coefficients were applied using band math to generate clay contents for each pixel. The resulting image is shown as gray scale for clay content (Figure 7b.)⁵³.

3. CONCLUSION

The advantages of hyperspectral imagery include the selection of specific bands for indexes, and the use of the wide range of spectroscopy analyses. Laboratory and field spectroscopic techniques were described that have demonstrated accuracies for identifying and quantifying vegetation and soil biophysical components can be or have been extended to field spectrometer, airborne and satellite imaging spectroscopy. These spectroscopic techniques will increase the information derived from a dense hyperspectral dataset for a variety of users investigating diverse applications using the same spectra.

Illustrated here are a few application examples for determining spectral bands useful in hyperspectral imaging spectrometers, as well as broad-band instruments, for precision agriculture in cotton production and soil management.

New analyses will give us water and nutrient stress information in time to respond without yield reduction. Indexes remain valuable tools for producers to evaluate the crop status, even with limited multi-band instruments. Plant and water indexes provided good predictors of cotton condition as harvest approached. With hyperspectral data, absorption modeling and strength measurements are viable means of estimating plant moisture and nutrient status. Measuring soil mineral abundance can be improved by accounting for the effect of soil moisture on the spectra.

Further research in use of imaging spectroscopy will lead to higher precision as producers refine their prescription models and application techniques. Our field data, and collaborators' airborne imagery and field data on plant mapping and canopy density, make a tremendous dataset that will take additional time to process. Continued investigations into irrigation scheduling using crop reflectance over a broad range of water contents, readiness for harvest aid chemical applications, and related field measurements will lead to improved accuracy in providing this key management information.

ACKNOWLEDGEMENTS

We would like to acknowledge the support of Cotton Incorporated; National Cotton Council, Cotton Foundation; and the UC Discovery Program. We wish to thank Dave Darling, and other students and staff in the Center for Spatial Technologies and Remote Sensing (CSTARS), University of California, Davis, who participated in the field and laboratory analyses, and support our information technology systems.

REFERENCES

1. National Research Council, *Precision agriculture in the 21st Century*. (National Academy Press, Washington, DC, 1997).
2. D. Jones and E. M. Barnes, "Fuzzy composite programming to combine remote sensing and crop models for decision support in precision crop management." *Agricultural Systems* **65**(3), 137-158 (2000).
3. M. S. Moran, Y. Inoue, and E. M. Barnes. "Opportunities and limitations for image-based remote sensing in precision crop management." *Remote Sensing of Environment* **61**, 319-346 (1997).
4. S. J. Maas, "Use of remotely-sensed information in agricultural crop growth models." *Ecological Modelling* **41**(3-4), 247-268 (1988).
5. R. Pearson, J. Grace, and G. May, "Real-time airborne agricultural monitoring." *Remote Sensing of Environment* **49**(3), 304-310 (1994).
6. C.-W. Chang, D. A. Laird, M. J. Mausbach, and C. R. Hurburgh, Jr., "Near-Infrared Reflectance Spectroscopy-Principal Components Regression Analyses of Soil Properties." *Soil Science Society of America Journal* **65**(2), 480-490 (2001).
7. A. Palacios-Orueta and S. L. Ustin, "Multivariate classification of soil spectra." *Remote Sensing of Environment* **57**(2), 108-118 (1996).
8. D. Haboudane, J. R. Miller, E. Pattey, P. J. Zarco-Tejada, and I. B. Strachan, "Hyperspectral vegetation indices and novel algorithms for predicting green LAI of crop canopies: modeling and validation in the context of precision agriculture." *Remote Sensing of Environment* **90**(3), 337-352 (2004).
9. J. W. Rouse, R. H. Haas, J. A. Schell, D. W. Deering, and J. C. Harlan., "Monitoring the vernal advancements and retrogradation of natural vegetation." (NASA/GSFC, Greenbelt, MD., 1974).
10. A. R. Huete, "A Soil-Adjusted Vegetation Index (SAVI)," *Remote Sensing of Environment* **25**(3), 295-309 (1988).
11. P. J. Zarco-Tejada, S. L. Ustin, and M. L. Whiting, "Temporal and spatial relationships between within-field yield variability in cotton and high-spatial hyperspectral remote sensing imagery." *Agronomy Journal* **97**(3), 641-653 (2005).
12. F. Tsai and W. Philpot, "Derivative analysis of hyperspectral data." *Remote Sensing of Environment* **66**, 41-51 (1998).
13. E. Ben-Dor and A. Banin, "Near infrared analysis (NIRA) as a method to simultaneously evaluate spectral featureless constituents in soils." *Soil Science* **159**(4), 259-270 (1995).
14. R. N. Clark, "Spectroscopy of rocks and minerals, and principles of spectroscopy." in *Remote Sensing for the Earth Sciences*, Third Edition ed., A. N. Rencz, ed. (John Wiley & Sons, Inc, New York, 1999), pp. 3-58.
15. R. N. Clark and T. L. Roush, "Reflectance spectroscopy: Quantitative analysis techniques for remote sensing applications." *Journal of Geophysical Research* **89**(B7), 6329-6340 (1984).

16. R. N. Clark, G. A. Swayze, K. E. Livo, R. F. Kokaly, S. J. Sutley, J. B. Dalton, R. R. McDougal, and C. A. Gent, "Imaging spectroscopy: Earth and planetary remote sensing with the USGS Tetracorder and expert systems." *Journal of Geophysical Research* **108**(E12), 5-1 - 5-44 (2003).
17. R. F. Kokaly and R. N. Clark, "Spectroscopic determination of leaf biochemistry using band-depth analysis of absorption features and stepwise multiple linear regression." *Remote Sensing of Environment* **67**, 267-287 (1999).
18. P. J. Curran, J. L. Dungan, and D. L. Peterson, "Estimating the foliar biochemical concentration of leaves with reflectance spectrometry: Testing the Kokaly and Clark methodologies." *Remote Sensing of Environment* **76**(3), 349-359 (2001).
19. G. F. Bonham-Carter, "Numerical procedures and computer program for fitting an inverted Gaussian Model to vegetation reflectance data." *Computers & Geoscience* **14**, 339-356 (1988).
20. J. R. Miller, E. W. Hare, and J. Wu, "Quantitative characterization of the vegetation red edge reflectance 1. An inverted-Gaussian reflectance model." *International Journal of Remote Sensing* **11**(10), 1755-1773 (1990).
21. J. M. Sunshine, C. M. Pieters, and S. F. Pratt, "Deconvolution of mineral absorption bands - an improved approach." *Journal of Geophysical Research-Solid Earth and Planets* **95**(B5), 6955-6966 (1990).
22. E. R. Stoner and M. F. Baumgardner, "Characteristic variations in reflectance of surface soils." *Soil Science Society of America Journal* **45**, 1161-1165 (1981).
23. M. F. Baumgardner, L. F. Silva, L. L. Biehl, and E. R. Stoner, "Reflectance properties of Soils." *Advances in Agronomy* **38**, 1-44 (1985).
24. T. L. Henderson, M. F. Baumgardner, D. P. Franzmeier, D. E. Stott, and D. C. Coster, "High dimensional reflectance analysis of soil organic matter." *Soil Science Society of America Journal* **56**, 865-872 (1992).
25. T. L. Coleman and O. L. Montgomery, "Soil moisture, organic matter, and iron content effect on the spectral characteristics of selected vertisols and alfisols in Alabama." *Photogrammetric Engineering and Remote Sensing* **53**(12), 1659-1663 (1987).
26. K. D. Shepherd and M. G. Walsh, "Development of reflectance spectral libraries for characterization of soil properties." *Soil Science Society of America Journal* **66**, 988-998 (2002).
27. T. Wassenaar, P. Andrieux, F. Baret, and J. M. Robbez-Masson, "Soil surface infiltration capacity classification based on the bi-directional reflectance distribution function sampled by aerial photographs. The case of vineyards in a Mediterranean area." *Catena* **62**(2-3), 94-110 (2005).
28. A. H. Al-Abbas, P. H. Swain, and M. F. Baumgardner, "Relating organic matter and clay content to the multispectral radiance of soils." *Soil Science* **114**, 477-485 (1972).
29. P. A. Agbu and E. Nizeyimana, "Comparisons between spectral mapping units derived from SPOT image texture and field soil map units." *Photogrammetric Engineering and Remote Sensing* **57**, 397-405. (1991).
30. P. J. Curran, "The use of polarized panchromatic and false-color infrared film in the monitoring of soil surface moisture." *Remote Sensing of Environment* **8**, 249-266 (1979).
31. K. A. Sudduth and J. W. Hummel, "Evaluation of reflectance methods for soil organic matter sensing." *Transactions of the ASAE* **34**, 1900-1909 (1991).
32. M. P. F. Fontes and I. A. Carvalho, Jr., "Color attributes and mineralogical characteristics, evaluated by radiometry, of highly weathered tropical soils." *Soil Science Society of America Journal* **69**(4), 1162-1172 (2005).
33. M. L. Whiting, L. Li, and S. L. Ustin, "Predicting water content using Gaussian model on soil spectra." *Remote Sensing of Environment* **89**(4), 535-552 (2004).
34. J.-L. Rougean and F. M. Breon, "Estimating PAR absorbed by vegetation from bidirectional reflectance measurements." *Remote Sensing of Environment* **51**, 375-384 (1995).
35. J. Chen, "Evaluation of vegetation indices and modified simple ratio for boreal applications." *Canadian Journal of Remote Sensing* **22**, 229-242 (1996).
36. C. S. T. Daughtry, C. L. Walthall, M. S. Kim, E. Brown de Colstoun, and J. E. M. III, "Estimating corn leaf chlorophyll concentration from leaf and canopy reflectance." *Remote Sensing of Environment* **74**, 229-239 (2000).
37. F. Baret, G. Guyot, and D. J. Major, "TSAVI: a vegetation index which minimizes soil brightness effects on LAI and APAR estimation." presented at the Proceedings of the 12th Canadian Symposium on Remote Sensing, IGARRS'90,, Vancouver, BC, Canada, 10-14 July, 1989.
38. J. Qi, A. Chehbouni, A. R. Huete, Y. H. Kerr, and S. Sorooshian, "A modified Soil Adjusted Vegetation Index." *Remote Sensing of Environment* **48**(2), 119-126 (1994).

39. G. Rondeaux, M. Steven, and F. Baret, "Optimization of soil-adjusted vegetation indices." *Remote Sensing of Environment* **55**(2), 95-107 (1996).
40. D. Haboudane, J. R. Miller, N. Tremblay, P. J. Zarco-Tejada, and L. Dextraze, "Integration of hyperspectral vegetation indices for prediction of crop chlorophyll content for application to precision agriculture." *Remote Sensing of Environment* **81**, 416-426 (2002).
41. N. H. Broge and E. Leblanc, "Comparing prediction power and stability of broadband and hyperspectral vegetation indices for estimation of green leaf area index and canopy chlorophyll density." *Remote Sensing of Environment* **76**, 156-172 (2000).
42. J. A. Gamon, J. Peñuelas, and C. B. Field, "A narrow-waveband spectral index that tracks diurnal changes in photosynthetic efficiency." *Remote Sensing of Environment* **41**, 35-44 (1992).
43. C. S. T. Daughtry, J. E. McMurtrey, E. W. Chappelle, W. P. Dulaney, J. R. Irons, and M. B. Satterwhite, "Potential For Discriminating Crop Residues From Soil By Reflectance and Fluorescence." *Agronomy Journal* **87**(2), 165-171 (1995).
44. B. Gao, "NDWI--A normalized difference water index for remote sensing of vegetation liquid water from space." *Remote Sensing of Environment* **58**(3), 257-266 (1996).
45. P. J. Zarco-Tejada, C. A. Rueda, and S. L. Ustin, "Water content estimation in vegetation with MODIS reflectance data and model inversion methods." *Remote Sensing of Environment* **85**(1), 109-124 (2003).
46. R. Fensholt and I. Sandholt, "Derivation of a shortwave infrared water stress index from MODIS near- and shortwave infrared data in a semiarid environment." *Remote Sensing of Environment* **87**, 111-121 (2003).
47. J. Peñuelas, J. Piñol, R. Ogaya, and I. Filella, "Estimation of plant water concentration by the reflectance Water Index (R900/ R970)." *International Journal of Remote Sensing* **18**, 2869-2875 (1997).
48. L. S. Galvao, M. A. Pizarro, and J. C. N. Epiphanyo, "Variations in reflectance of tropical soils: spectral-chemical composition relationships from AVIRIS data." *Remote Sensing of Environment* **75**, 245-255 (2001).
49. A. Palacios-Orueta, J. E. Pinzon, S. L. Ustin, and D. A. Roberts, "Remote sensing of soil properties in the Santa Monica mountains: II. Hierarchical foreground and background analysis." *Remote Sensing of Environment* **68**, 138-151 (1999).
50. F. A. Kruse, A. B. Lefkoff, and J. B. Dietz, "Expert system-based mineral mapping in northern death valley, California/Nevada, using the Airborne Visible/Infrared Imaging Spectrometer (AVIRIS)." *Remote Sensing of Environment* **44**(2-3), 309-336 (1993).
51. G. R. Taylor, A. H. Mah, F. A. Kruse, K. S. Kiereinyoung, R. D. Hewson, and B. A. Bennett, "Characterization of saline soils using airborne radar imagery." *Remote Sensing of Environment* **57**(3), 127-142 (1996).
52. F. van der Meer, "Analysis of spectral absorption features in hyperspectral imagery." *International Journal of Applied Earth Observation and Geoinformation* **5**, 55-68 (2004).
53. M. L. Whiting, A. Palacios-Orueta, L. Li, and S. L. Ustin, "Light absorption model for water content to improve soil mineral estimates in hyperspectral imagery.," presented at the Pecora 16: Global Priorities in Land Remote Sensing, Sioux Falls, South Dakota, October 23-27, 2005, 2005.
54. F. van der Meer and W. Bakker, "Cross correlogram spectral matching: Application to surface mineralogical mapping by using AVIRIS data from Cuprite, Nevada." *Remote Sensing of Environment* **61**(3), 371-382 (1997).
55. S. A. Bowers and R. J. Hanks, "Reflection of radiant energy from soils." *Soil Science* **100**(2), 130-138 (1965).
56. W. Liu, F. Baret, X. Gu, Q. Tong, L. Zheng, and B. Zhang, "Relating soil surface moisture to reflectance." *Remote Sensing of Environment* **81**, 238-246 (2002).
57. D. B. Lobell and G. P. Asner, "Moisture effects on soil reflectance." *Soil Science Society of America Journal* **66**, 722-727 (2002).
58. J. A. M. Demattê, A. A. Sousa, M. C. Alves, and M. R. Nanni, "Determining soil water status and other soil characteristics by spectral proximal sensing." *Geoderma* (in press).
59. G. I. Metternicht and J. A. Zinck, "Remote sensing of soil salinity: potentials and constraints." *Remote Sensing of Environment* **85**(1), 1-20 (2003).
60. G. I. Metternicht and J. A. Zinck, "Modelling salinity-alkalinity classes for mapping salt-affected topsoils in the semiarid valleys of Cochabamaba (Bolivia)." *ITC Journal* **2**, 125-135 (1996).
61. R. E. Plant, D. S. Munk, B. R. Roberts, R. L. Vargas, D. W. Rains, R. L. Travis, and R. B. Hutmacher, "Relationships between remotely sensed reflectance data and cotton growth and yield." *Transactions of the American Society of Agricultural Engineers* **43**(3), 535-546 (2000).

62. R. L. Dehaan and G. R. Taylor, "Field-derived spectra of salinized soils and vegetation as indicators of irrigation-induced soil salinization." *Remote Sensing of Environment* **80**(3), 406-417 (2002).
63. M. S. Moran, S. J. Maas, V. C. Vanderbilt, E. M. Barnes, S. N. Miller, and T. R. Clarke, "Application of imagebased remote sensing to irrigated agriculture." in *Manual of Remote Sensing, Remote Sensing for Natural Resource Management and Environmental Monitoring*, S. L. Ustin, ed. (ASPRS and John Wiley and Sons, New York, 2004), pp. 617-676.
64. C. M. Champagne, K. Staenz, A. Bannari, H. McNairn, and J.-C. Deguise, "Validation of a hyperspectral curve-fitting model for the estimation of plant water content of agricultural canopies." *Remote Sensing of Environment* **87**(2-3), 148-160 (2003).
65. H. G. Downing, G. A. Carter, K. W. Holladay, and W. G. Cibula, "The radiative-equivalent water thickness of leaves." *Remote Sensing of Environment* **46**(1), 103-107 (1993).
66. C. J. Tucker, "Remote sensing of leaf water content in the near infrared." *Remote Sensing of Environment* **10**(1), 23-32 (1980).
67. L. Serrano, S. L. Ustin, D. A. Roberts, J. A. Gamon, and J. Peñuelas, "Deriving water content of chaparral vegetation from AVIRIS data." *Remote Sensing of Environment* **74**, 570-581 (2000).
68. S. L. Ustin, D. A. Roberts, J. Pinzon, S. Jacquemoud, M. Gardner, G. Scheer, C. M. Castaneda, and A. Palacios-Orueta, "Estimating Canopy Water Content of Chaparral Shrubs Using Optical Methods." *Remote Sensing of Environment* **65**(3), 280-291 (1998).
69. E. B. Knipling, "Physical and physiological basis for the reflectance of visible and near-infrared radiation from vegetation." *Remote Sensing of Environment* **1**(3), 155-159 (1970).
70. P. S. Thenkabail, R. B. Smith, and E. De Pauw, "Hyperspectral vegetation indices and their relationships with agricultural crop characteristics." *Remote Sensing of Environment* **71**(2), 158-182 (2000).
71. G. A. Blackburn, "Quantifying chlorophylls and carotenoids at leaf and canopy scales: an evaluation of some hyperspectral approaches." *Remote Sensing of Environment* **66**(3), 273-285 (1998).
72. V. C. LaCapra, J. M. Melack, M. Gastil, and D. Valeriano, "Remote sensing of foliar chemistry of inundated rice with imaging spectrometry." *Remote Sensing of Environment* **55**(1), 50-58 (1996).
73. G. A. Carter and R. L. Miller, "Early detection of plant stress by digital imaging within narrow stress-sensitive wavebands." *Remote Sensing of Environment* **50**(3), 295-302 (1994).
74. G. A. Carter and A. K. Knapp, "Leaf optical properties in higher plants: linking spectral characteristics to stress and chlorophyll concentration." *American Journal of Botany* **88**(4), 677-684 (2001).
75. J. Willers, J. Jenkins, W. Ladner, P. Gerard, D. Boykin, K. Hood, P. McKibben, S. Samson, and M. Bethel, "Site-specific approaches to cotton insect control. sampling and remote sensing analysis techniques." *Precision Agriculture* **6**(5), 431-452 (2005).
76. Z. Qin and M. Zhang, "Detection of rice sheath blight for in-season disease management using multispectral remote sensing." *International Journal of Applied Earth Observation and Geoinformation* **7**(2), 115-128 (2005).
77. M. Zhang, X. Liu, and M. Oneill, "Spectral discrimination of phytophthora infestans infection on tomatoes based on principal component and cluster analyses." *International Journal of Remote Sensing* **23**, 1095-1107 (2002).
78. F. A. Kruse, A. B. Lefkoff, J. W. Boardman, K. B. Heidebrecht, A. T. Shapiro, P. J. Barloon, and A. F. H. Goetz, "The spectral image processing system (SIPS)--interactive visualization and analysis of imaging spectrometer data." *Remote Sensing of Environment* **44**(2-3), 145-163 (1993).
79. S. L. Ustin, D. Darling, S. Kefauver, J. Greenberg, Y.-B. Cheng, and M. L. Whiting, "Remotely sensed estimates of crop water demand." presented at the International Symposium on Optical Science and Technology, 49th Annual Meeting, Denver, CO. August 2-6, 2004, 2004.
80. P. L. Nagler, Y. Inoue, E. P. Glenn, A. L. Russ, and C. S. T. Daughtry, "Cellulose absorption index (CAI) to quantify mixed soil-plant litter scenes." *Remote Sensing of Environment* **87**(2-3), 310-325 (2003).
81. T. G. Chrien, R. O. Green, J. Boardman, B. Chippendale, C. J. Chovit, M. Eastwood, J. A. Faust, M. Finn, P. Hall, J. Hobrook, J. Houston, C. Kurzweil, J. Longenecker, J. Raney, C. Sarture, and G. Tuell, "Operation of NASA's Airborne Visible/Infrared Imaging Spectrometer (AVIRIS) on a NOAA Twin Otter: Program Overview." presented at the Eighth JPL Airborne Earth Science Workshop, Jet Propulsion Laboratory, California Institute of Technology, Pasadena, CA, February 10-11, 1999, 1999.